Generation of few-cycle laser pulses by coherent synthesis based on a femtosecond Yb-doped fiber laser amplification system

Aichen Ge (葛爱晨), Bowen Liu (刘博文)*, Wei Chen (陈 伟), Haochen Tian (田昊晨), Youjian Song (宋有建), Lu Chai (柴 路), and Minglie Hu (胡明列)

Ultrafast Laser Laboratory, School of Precision Instrument and Optoelectronics Engineering, Key Laboratory of Optoelectronic Information Technology (Ministry of Education), Tianjin University, Tianjin 300072, China

**Corresponding author: bwliu@tju.edu.cn*

Received September 30, 2018; accepted January 15, 2019; posted online April 1, 2019

We demonstrate a coherent synthesis system based on femtosecond Yb-doped fiber laser technology. The output pulse of the amplification system is divided into two replicas and seeded into photonic crystal fibers of two parallel branches for nonlinear pulse compression. Because of the different nonlinear dynamics in the photonic crystal fibers, the compressed pulses show different spectra, which can be spliced to form a broad coherent spectrum. The integrated timing jitter between the pulses of two branches is less than one tenth of an optical cycle. By coherently synthesizing pulses from these two branches, 8 fs few-cycle pulses are produced.

OCIS codes: 140.3490, 060.2420, 060.3735, 060.2370.

doi: 10.3788/COL201917.041403.

Ultrashort laser pulses have become an ideal tool for both fundamental research and industrial applications because of their excellent time resolution and high peak power. Since the invention of the mode-locked laser, the desire for shorter possible pulses has been motivating the research interest of generating broad coherent spectra all the time[1–3]. However, the output pulse duration from an individual mode-locked laser is mainly limited by the gain bandwidth of its active laser medium, especially for fiber lasers, which can generate high-average-power pulse trains with a compact and robust structure[4,5]. To overcome this drawback, extracavity nonlinear pulse compression, such as dechirping the pulse spectrally broadened by self-phase modulation (SPM) and soliton-self-frequency shift (SSFS), is commonly applied to extend the pulse spectrum for few-cycle duration[6,7]. Unfortunately, the nonlinear chirp induced by the SPM makes it difficult to obtain a nearly transform-limited (TL) pulse, unless sophisticated feedback to control the spectral phase is utilized. Although a nearly TL pulse can be directly generated from the SSFS process, the output pulse duration is always limited to approximately tens of femtoseconds. In view of the success of optical parametric amplification[8,9] and optical parametric oscillator technology[10,11] in the Ti:sapphire system, they can also be used in the fiber laser system to generate broadband tunable few-cycle pulses[12,13]. But, the complex spatial optical paths make facilities difficult to build and control, moreover losing the advantages of fiber systems.

Coherent synthesis based on femtosecond fiber laser system offers another promising route to achieve broad coherent spectra for few-cycle laser pulses. There are two common methods of coherent synthesis. One is locking the relative pulse repetition rate and carrier-envelope offset (CEO) frequency between two independent mode-locked fiber lasers[14–16]. In 2012, Cox *et al.* realized the synthesis of a passively mode-locked Ti:sapphire laser and a fiber supercontinuum[17]. In 2015, Fong *et al.* locked the relative carrier-envelope phase between ultrafast Yb and Er fiber laser systems[18]. For synthesis of two separate mode-locked lasers, sophisticated phase locking is necessary and makes the system difficult to operate. The other method is to synthesize multiple branches of pulses, which share the same seed source. The pulses of different branches show different spectra induced by different nonlinear frequency conversion processes and are coherently combined[19–21]. Compared with synthesis of two separate laser sources, the greatest advantage of this method is that active locking of the repetition rate and relative CEO frequency is not necessary. It is because pulse trains of different branches keep the same repetition rate of the seed source, and new spectral components generated by nonlinear frequency conversion preserve the CEO frequency of the pump pulse. With this method, the shorter coherently combined pulses can be obtained in a much simpler system. In 2009, Krauss *et al.* obtained single-cycle pulses by coherently synthesizing dispersive waves and Raman solitons generated in different highly nonlinear fibers (HNFs) based on an Er-doped fiber laser system[19]. To generate the short synthesized pulse with high temporal quality, this kind of coherent combination needs the short duration of pulses in each branch, as well as a spectral splice without a gap. When the duration of the combined pulse is nearly few-cycle, the low relative timing jitter (RTJ) between pulses of different branches is important. Due to interaction between the relative intensity noise (RIN) of pulses and the dispersion of fibers, the timing jitter of output

 © 2019 Chinese Optics Letters

pulses will be enhanced[22]. Therefore, the seed source should output pulses with enough average power to avoid further amplification in branches because different fiber amplifiers induce different RIN and further increase the RTJ.

In this Letter, we present a coherent synthesis system based on a home-built Yb-doped fiber amplification system. Self-similar amplification is employed in a tailor-cut fiber amplifier, to output ~70 fs pulses with a high average power. By taking advantage of the high average power of this laser pulse source, further amplification is not necessary in each branch. It avoids the individual amplification noise. Moreover, <100 fs pulse duration benefits the following nonlinear pulse compression to obtain high-quality short parent pulses for few-cycle pulse synthesis. The parent pulses of both branches are generated via dechirping the pulses spectrally broadened by SPM and dispersive waves radiated from high-order soliton fission. The spectra of both parent pulses can overlap, benefitting the temporal quality of synthesized pulses, which cannot be obtained by combining the dispersive wave and soliton. On the premise of enough bandwidths of the parent pulses, we minimize the length of the HNFs to maintain the coherence and low RTJ of the parent pulses[23,24]. Indeed, the integrated timing jitter of the pulses of both branches is less than one tenth of an optical cycle[25], although no active feedback stabilization of the relative timing is implemented. After coherent synthesis, 8 fs synthesized pulses with high temporal quality are obtained. This is the shortest coherently synthesized pulse based on a Yb-doped fiber laser system as far as we know.

The experimental scheme is shown in Fig. 1. The Yb-doped fiber femtosecond laser amplification system consists of an oscillator, a pre-amplifier, a pre-shaper, a main amplifier, and a compressor. The oscillator is a dissipative-soliton mode-locked Yb-doped fiber laser. It outputs ~1 ps pulses at a 150 MHz repetition rate. Then, the average power of the pulses is amplified to ~100 mW in the pre-amplifier. In nonlinear pulse compression, the shorter pump pulse duration ensures the shorter derived pulse. Thus, the temporal breathing self-similar pulse

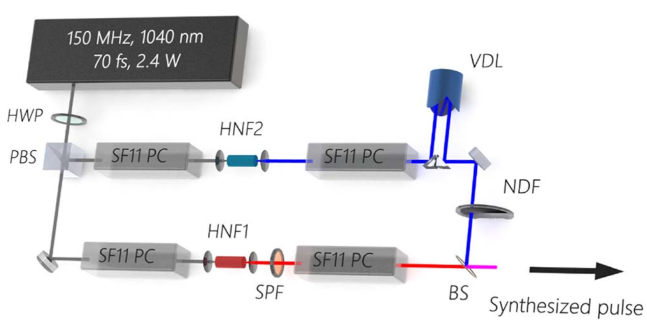

Fig. 1. Schematic of coherent synthesis system. HWP, half-wave plate; PBS, polarization beam splitter; SF11 PC, SF11 prism compressor; SPF, short-pass filter; VDL, variable delay line; NDF, neutral density filter; BS, beam splitter.

evolution is implemented in the main amplifier for a broad bandwidth and linear chirp of the output pulse by optimizing the pre-chirp and central wavelength of the seed pulse with the pre-shaper[26]. After compression, the amplification system outputs 70 fs nearly TL pulses with 2.4 W average power. Afterwards, the output pulse train is split into two branches by a half-wave plate (HWP) and a polarization beam splitter (PBS). In each branch, a pair of SF11 prisms is utilized to control the pre-chirp of the pulses before being coupled into the HNFs, so as to optimize the nonlinear evolution in the HNF. Two kinds of photonic crystal fibers (PCFs) from NKT Photonics are used as the HNFs for different nonlinear processes. In one branch, the PCF (SC-3.7-975, HNF1) has one zero-dispersion wavelength around 975 nm, which is suitable for generating typical high-order soliton fission and dissipative wave radiation processes. TL pulses with 5.7 nJ energy are coupled into 22 mm HNF1. A short-pass filter (cutoff wavelength 1000 nm) isolates the long-wavelength components of the output pulse. The short-wavelength part generated by the dispersive wave is dechirped by an SF11 prism pair. In the other branch, the all-normal dispersion fiber (NL-1050-NEG-1, HNF2) is employed for only SPM-based spectral broadening, because this fiber shows a flat and normal group-velocity dispersion curve in the 1000–1100 nm wavelength range. The positively chirped pulses with 10.3 nJ energy are coupled into 20 mm HNF2, and the output pulses are dechirped by the following SF11 prism pair to the shortest pulse duration. The time delay Δt between the parent pulses of the two branches is adjusted by a piezo-controlled retroreflector. The moving resolution of the piezo is 20 nm (~0.06 fs temporal resolution), which is precise enough to control the delay time. A neutral density filter (NDF) is equipped to adjust the parent pulse energy ratio of the two branches. In the end, the parent pulses are combined collinearly by a film beam splitter.

In order to analyze the spectral broadening process and optimize the fiber length, simulation of pulse nonlinear evolution in both HNFs is performed first, as shown in Figs. 2(a) and 2(b). We used the split-step Fourier transform method to solve the nonlinear Schrödinger equation and employed a self-adaptive algorithm to improve simulation efficiency[27]. In the simulation, the pump pulse is described by the temporal and spectral parameters measured in the experiment. The dispersion curve and nonlinearity parameters of the fibers are based on the data sheet from the manufacturer. For the case in HNF1, the dynamics is featured by high-order soliton fission and dispersive wave radiation. The high-order soliton breaks into several individual solitons, and then they redshift due to intrapulse stimulated Raman scattering. Meanwhile dispersive waves are radiated on the short-wavelength side of the zero-dispersion wavelength. In this evolution, the bandwidths of the dispersive wave around 875 nm and the soliton around 1350 nm are both broad enough. Compared with the soliton, the spectral components of the dispersive wave can be well spliced with the spectrum of the output

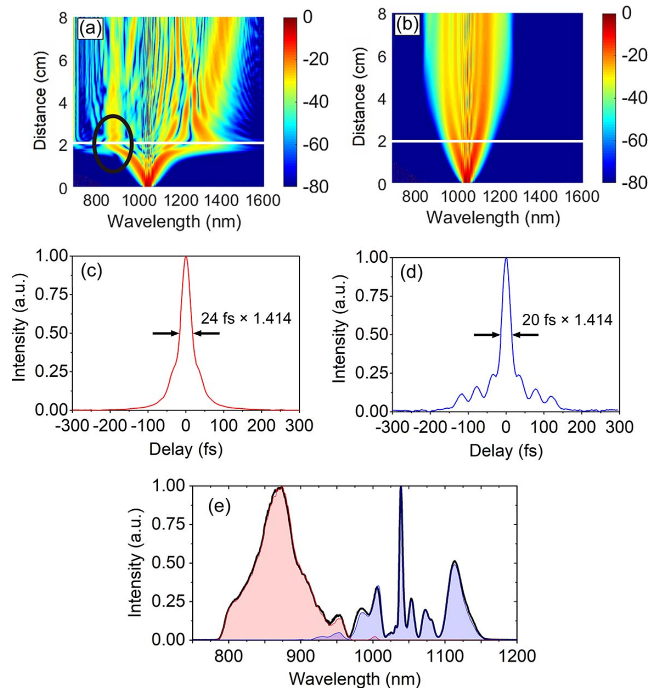

Fig. 2. Spectral evolution in (a) HNF1 and (b) HNF2, where the white lines are the optimum length of the nonlinear fibers for pulse output, and the red circle indicates the dispersive wave generated in HNF1. The autocorrelation traces of (c) dechirped dispersive wave from HNF1 and (d) dechirped pulses output from HNF2. (e) Measured spectra of pulses output from HNF1 (red), dispersive wave output from HNF2 (blue), and the coherently synthesized pulse (black line).

pulse from HNF2, avoiding the spectral gap of the combined pulse. According to the Fourier relation, depressing the pedestal of the combined pulse can benefit from dispersive wave extraction for coherent synthesis. After the pulse propagates the leading 22 mm in HNF1, the dispersive wave is completely formed, and its bandwidth cannot be extended with further propagation. In addition, a longer propagation distance will increase the timing jitter of the Raman soliton as well as the dispersive wave[22,23], which can enlarge the RTJ between both branches. Thus, we can only use a 22 mm HNF1 segment to obtain a broadband dispersive wave. The dispersive wave shows a ∼80 nm bandwidth (corresponding to a ∼20 fs TL pulse duration) and can be compressed to a nearly TL pulse. The spectral broadening process in HNF2 is dominated by SPM, which can preserve linear chirp over a large central region of the pulse, resulting in a high compression ratio[28]. After the first ∼20 mm propagation in HNF2, the pulse bandwidth is extended to ∼150 nm (corresponding to a ∼12 fs TL pulse duration). With a prism compressor, we can obtain a ∼22 fs output pulse. It is short enough to support the following coherent synthesis towards few-cycle pulses. However, further propagation will introduce more high-order chirp on the edges of the pulse temporal profile, which is difficult to compensate for by a common compressor.

According to the numerical result, 22 mm HNF1 and 20 mm HNF2 are adopted in the experiment. The experimental results are shown in Fig. 2. The spectrum of the dispersive wave from HNF1 is smooth and Gaussian-like. In addition, its chirp is nearly linear. As a result, the dispersive wave can be dechirped to a nearly TL pulse, and the full-width at half-maximum (FWHM) of the pulses autocorrelation (AC) trace is 35 fs, corresponding to 24 fs pulse duration when approximated to Gaussian pulses. But, the mismatch of high-order dispersion between HNF1 and the prism pair induces the pedestal on the pulse. The spectrum of the pulse output from HNF2 presents a typical SPM-induced oscillatory structure. After compression, the FWHM of the pulse autocorrelation trace is as short as 28 fs, corresponding to 20 fs pulse duration when approximated to Gaussian pulses. The autocorrelation trace shows sub-pulses on the pedestal, which are induced by the multi-peak structure of the spectrum. The spectra of both pulses overlap around 970 nm. These two pulses are employed as parent pulses for the synthesis.

To demonstrate that the RTJ between the two branches is low enough for coherent synthesis, the timing jitter of the parent pulse in each branch is separately measured by optical cross-correlations. In the measurement, the pump pulse from the amplification system is used as the reference pulse. Type-I phase-matched 2 mm beta-barium borate (BBO) is applied for sum-frequency generation from the pump and parent pulses in cross-correlation. We have also measured the RIN of the pump pulses for comparison [Fig. 3(a)]. The integrated RIN is 0.23%. The different dynamics in the two HNFs makes the timing jitter spectra of the two branches different.

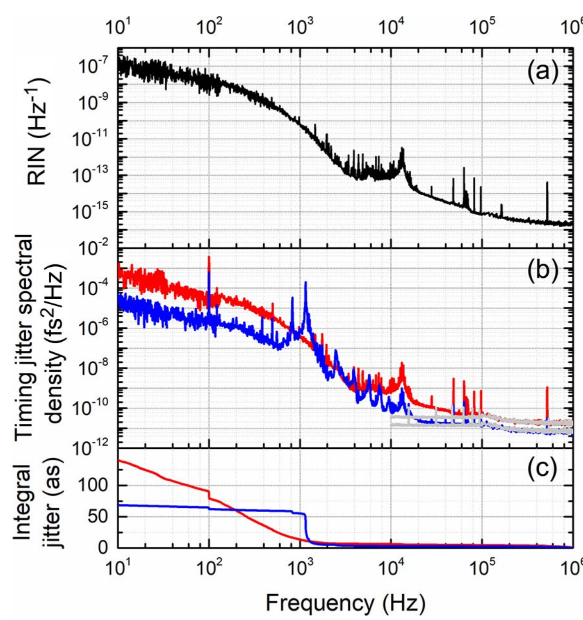

Fig. 3. (a) Relative intensity noise of pump pulses. (b) Timing jitter spectrum of dispersive wave from HNF1 (red) and pulses from HNF2 (blue), and the gray lines are the noise floors. (c) Integrated RMS timing jitter of dispersive wave from HNF1 (red) and pulses from HNF2 (blue).

In HNF1, the energy fluctuation of the pump pulse can be converted into a central wavelength variation of solitons through the SSFS process[22]. The solitons with different central wavelengths propagate at different group velocities because of the fiber dispersion. So, the RIN of the pump pulses is transferred into the timing jitter of the Raman soliton. Furthermore, this timing jitter accumulates during the propagation of the soliton in the fiber. Meanwhile, the central wavelength of the dispersive wave is determined by the peak power and central wavelength of the soliton, according to the phase matching condition[23]. Therefore, the central wavelength variation of the soliton is transferred to the dispersive wave, and the RIN of pump pulses is also coupled with the timing jitter of the dispersive wave.

In the experiment, the timing jitter spectrum of the dispersive wave pulse output from HNF1 is measured, as shown in Fig. 3(b). Clearly, the timing jitter curve follows exactly the same frequency dependency as the pump pulse's RIN curve, implying that the timing jitter of the dispersive wave is mainly induced by the pump pulse's RIN. For the case of nonlinear dynamics in HNF2, SPM dominates the spectral broadening process. The pulse spectrum is extended symmetrically during pulse propagation, avoiding the center wavelength change. So, the RIN of the pump pulse cannot be coupled into the timing jitter of the output pulse, but through the dispersion of fiber. Although a peak emerges near 1 kHz, free of RIN-coupled timing jitter, it still makes the timing jitter of the pulse output from HNF2 lower than that of the dispersive wave pulse obtained from HNF1, which is obviously in the low frequency range. The root mean square (RMS) timing jitters [Fig. 3(c)] integrated from 10 Hz to 1 MHz are 69 and 140 as for the parent pulses from HNF2 and HNF1, respectively. This results in the upper limit of the integrated RMS timing jitter between the two parent pulses of 156, as is lower than 1/10 of the optical cycle. The measurement noise floors are 3.74×10^{-11} fs^2/Hz and 1.43×10^{-11} fs^2/Hz for HNF1 and HNF2, corresponding to 6.11×10^{-3} as/sqrt(Hz) and 3.78×10^{-3} as/sqrt(Hz) resolution, respectively[29].

The time delay Δt between parent pulses of the two branches is controlled by a retroreflector on a variable delay stage, the position of which is fine-tuned by a piezoelectric transducer. Figure 4(a) shows the AC traces for different Δt. When the value of Δt is larger than 40 fs, there are obviously two parts. One part is a superposition of the autocorrelations of two parent pulses appearing in the central region, and the other part is their cross-correlation around the point with an autocorrelator delay time of $\pm\Delta t$. As Δt is decreased from 40 fs, the cross-correlation gets close to the center of the trace and finally cannot be distinguished from the central part. Meanwhile, the amplitude of the central peak of the AC trace begins to rise because two parent pulses temporally overlap step by step and interference occurs. When Δt is zero, the optimum relative temporal position between the two pulses,

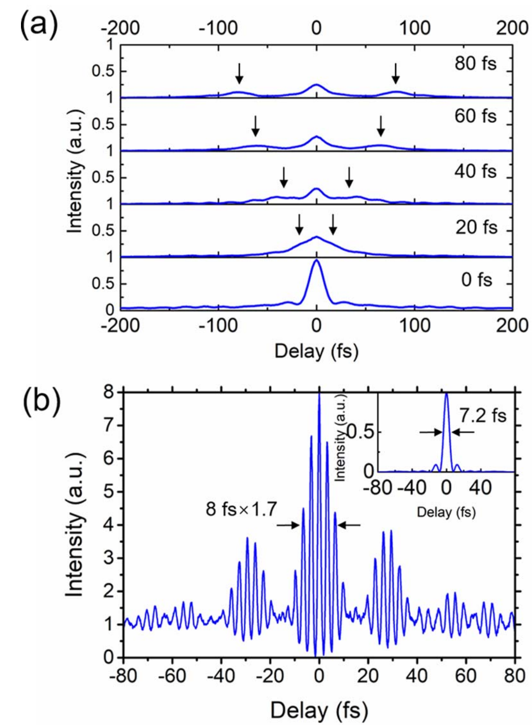

Fig. 4. (a) Evolution of the autocorrelator trace with delay between two pulses. (b) Fringe-resolved autocorrelator trace of the synthesized pulses. Inset figure is the intensity of the TL pulse obtained from the synthesized spectrum shown in Fig. 2(e).

constructive interference of the central fields of both pulses, arises. In the experiment, the NDF is applied to adjust the energy ratio between two branch parent pulses for high-quality synthesized pulses. The optimum synthesized pulses can be obtained when the energy ratio is 1:1. The spectrum of the synthesized pulse is shown in Fig. 2(e). The amplitude of the coherently synthesized pulse is measured by a home-built fringe-resolved autocorrelator, as shown in Fig 4(b). The FWHM of fringe-resolved autocorrelator trace is 13 fs. When pulses are approximated to Gaussian pulses, the deconvolution factor is 1.7[30]. Thus, the FWHM of the pulse is 8 fs. The intensity of the TL pulse obtained from the synthesized spectrum [Fig. 2(e)] is shown in the inset of Fig. 4(b). The FWHM of the TL pulse is 7.2 fs, which is close to the duration of the synthesized pulse. A series of secondary pulses emerges at the two sides of the main pulse, which cannot be cancelled by the interference of two parent pulses in the time domain. The pulse energy of the synthesized few-cycle pulse is 0.4 nJ.

In conclusion, coherent synthesis based on a Yb-doped fiber femtosecond laser amplification system is demonstrated. The high output power of the seed pulse source benefits the following coherent combination. There is no further amplification in branches avoiding the different RIN between pulses of two branches. Two branch parent pulses are obtained via dechirping the dispersive wave and the pulse spectrally broadened by SPM. According to the simulation result, the lengths of the HNFs are optimized to ensure efficient spectral broadening, as well as to minimize the accumulation of timing jitter. The integrated RMS timing jitters of two branches measured are less than 1/10 of an optical cycle, and low enough to support a few-cycle pulse duration. When the two parent pulses are coherently well synthesized, 8 fs pulses are generated. In the future, the PCFs can be further optimized to generate dispersive waves with a higher energy, and more than two branches can be utilized to obtain an octave spectrum for coherent synthesis for single-cycle pulses.

The work is partially supported by the National Natural Science Foundation of China (NSFC) (Nos. U1730115, 61535009, and 11527808) and the Open Fund of State Key Laboratory of High Field Laser Physics (Shanghai Institute of Optics and Fine Mechanics).

References

1. G. G. Paulus, F. Grasbon, H. Walther, P. Villoresi, M. Nisoli, S. Stagira, E. Priori, and S. De Silvestri, Nature **414**, 182 (2001).
2. K. Wang, X. Gu, Z. Zhang, Z. Yang, J. Liu, and S. Wang, Chin. Opt. Lett. **16**, 090401 (2018).
3. F. Feng and L. Bai, Chin. Opt. Lett. **16**, 063201 (2018).
4. B. Ortaç, A. Hideur, and M. Brunel, Opt. Lett. **29**, 1995 (2004).
5. W. Gao, G. Liu, and Z. Zhang, Chin. Opt. Lett. **16**, 111401 (2018).
6. S. Demmler, J. Rothhardt, A. M. Heidt, A. Hartung, E. G. Rohwer, H. Bartelt, J. Limpert, and A. Tünnermann, Opt. Express **19**, 20151 (2011).
7. A. Sell, G. Krauss, R. Scheu, R. Huber, and A. Leitenstorfer, Opt. Express **17**, 1070 (2009).
8. C. P. Hauri, P. Schlup, G. Arisholm, J. Biegert, and U. Keller, Opt. Lett. **29**, 1369 (2004).
9. S. Witte and K. S. E. Eikema, IEEE J. Sel. Top. Quantum Electron. **18**, 296 (2012).
10. S. C. Kumar, A. Esteban-Martin, T. Ideguchi, M. Yan, S. Holzner, T. W. Hänsch, N. Picqué, and M. Ebrahim-Zadeh, Laser Photon. Rev. **8**, L86 (2014).
11. R. A. McCracken and D. T. Reid, Opt. Lett. **40**, 4102 (2015).
12. J. Rothhardt, S. Hädrich, E. Seise, M. Krebs, F. Tavella, A. Willner, S. Düsterer, H. Schlarb, J. Feldhaus, J. Limpert, J. Rossbach, and A. Tünnermann, Opt. Express **18**, 12719 (2010).
13. N. Leindecker, A. Marandi, R. L. Byer, K. L. Vodopyanov, J. Jiang, I. Hartl, M. Fermann, and P. G. Schunemann, Opt. Express **20**, 7046 (2012).
14. R. K. Shelton, L.-S. Ma, H. C. Kapteyn, M. M. Murnane, J. L. Hall, and J. Ye, Science **293**, 1286 (2001).
15. T. R. Schibli, J. Kim, O. Kuzucu, J. T. Gopinath, S. N. Tandon, G. S. Petrich, L. A. Kolodziejski, J. G. Fujimoto, E. P. Ippen, and F. X. Kärtner, Opt. Lett. **28**, 947 (2003).
16. H. Tian, Y. Song, F. Meng, Z. Fang, M. Hu, and C. Wang, Opt. Lett. **41**, 5142 (2016).
17. J. A. Cox, W. P. Putnam, A. Sell, A. Leitenstorfer, and F. X. Kärtner, Opt. Lett. **37**, 3579 (2012).
18. B. Fong, W. Lin, S. Wu, J. Peng, W. Hsiang, and Y. Lai, Opt. Lett. **40**, 966 (2015).
19. G. Krauss, S. Lohss, T. Hanke, A. Sell, S. Eggert, R. Huberm, and A. Leitenstorfer, Nat. Photon. **4**, 33 (2009).
20. C. Manzoni, S.-W. Huang, G. Cirmi, P. Farinello, J. Moses, F. X. Kärtner, and G. Cerullo, Opt. Lett. **37**, 1880 (2012).
21. S. Huang, G. Cirmi, J. Moses, K. Hong, S. Bhardwaj, J. R. Birge, L. Chen, E. Li, B. J. Eggleton, G. Cerullo, and F. X. Kärtner, Nat. Photon. **5**, 475 (2011).
22. G. Zhou, M. Xin, F. X. Kärtner, and G. Chang, Opt. Lett. **40**, 5105 (2015).
23. J. M. Dudley, G. Genty, and S. Coen, Rev. Mod. Phys. **78**, 1135 (2006).
24. G. A. Nowak, J. Kim, and M. N. Islam, Appl. Opt. **38**, 7364 (1999).
25. C. Manzoni, O. D. Mucke, G. Cirmi, S. Fang, J. Moses, S. Huang, K. Hong, G. Cerullo, and F. X. Kartner, Laser Photon. Rev. **9**, 129 (2015).
26. S. Wang, B. Liu, C. Gu, Y. Song, C. Qian, M. Hu, L. Chai, and C. Wang, Opt. Lett. **38**, 296 (2013).
27. O. V. Sinkin, R. Holzlöhner, J. Zweck, and C. R. Menyuk, J. Lightwave Technol. **21**, 61 (2003).
28. A. M. Heidt, J. Opt. Soc. Am. B **27**, 550 (2010).
29. D. Hou, C.-C. Lee, Z. Yang, and T. R. Schibli, Opt. Lett. **40**, 13 (2015).
30. Z. G. Zhang, *Femtosecond Laser Technologies* (Science, 2011).